LAWRENCE
LIVERMORE
NATIONAL
LABORATORY

LLNL-JRNL-482515

Investigation of Large LGB Detectors for Antineutrino Detection

P. Nelson, N. Bowden

May 3, 2011

Nuclear Instruments and Methods A

Disclaimer

Investigation of Large LGB Detectors for Antineutrino Detection

P. Nelson[a,1], N. S. Bowden[*,b]

[a] *Department of Physics, Naval Postgraduate School, Monterey, CA 93943, USA*
[b] *Lawrence Livermore National Laboratory, Livermore, CA 94550, USA*

Abstract

A detector material or configuration that can provide an unambiguous indication of neutron capture can substantially reduce random coincidence backgrounds in antineutrino detection and capture-gated neutron spectrometry applications. Here we investigate the performance of such a material, a composite of plastic scintillator and $^{6}Li^{nat}_{6}Gd(^{10}BO_3)_3$:Ce (LGB) crystal shards of $\approx$ 1 mm dimension and comprising 1% of the detector by mass. While it is found that the optical propagation properties of this material as currently fabricated are only marginally acceptable for antineutrino detection, its neutron capture identification ability is encouraging.

Key words: thermal neutron detection, capture-gated neutron spectrometry

1. Introduction

Neutron detection systems incorporating a neutron capture agent or neutron capture indicating detector have many applications. These include, but are by no means limited to, thermal neutron detection (e.g. ^{3}He tubes), capture-gated fast neutron spectrometry [1], and reactor antineutrino detection [2, 3]. Materials or systems that provide an unambiguous indication of a neutron capture are to be preferred in all these applications, as this provides a means of rejecting background. In all of the applications listed above, γ-ray rejection is of high importance, while in antineutrino detection rejection of cosmogenic multiple neutron backgrounds could also be advantageous.

Considering the reactor antineutrino detection application more fully, most detectors employ the inverse beta decay interaction: $\bar{\nu}_e + p \rightarrow e^+ + n$, in which the final state positron and neutron typically have energies of a few MeV and a few keV, respectively. Observation of a scintillation light pulse from the positron slowing and annihilation followed by some indication of neutron capture 10s to 100s of μs later provides for a powerful means of uncorrelated (random) background rejection, and is closely analogous to the observation of recoil proton slowing followed by a neutron capture employed in the capture gating technique[2]. Many antineutrino detectors rely upon Gd-doped scintillators to provide that neutron capture indication, due to the large cross-section for and energetic $\approx$ 8 MeV gamma-ray shower

[*]Corresponding Author. Tel.: +1 925 422 4923.
Email address: nbowden@llnl.gov (N. S. Bowden)
[1]Present Address: United States Military Academy, West Point, NY 10996 USA
[2]Indeed, fast neutron slowing and capture is a major source of correlated background in antineutrino detectors.

released by neutron captures on ^{155}Gd and ^{157}Gd. Despite the powerful background rejection afforded by time-correlated detection, random coincidences of uncorrelated background gamma-rays can substantially exceed typical antineutrino interaction rates (100s-1000s per day), even in well shielded devices. A gamma-ray based neutron capture indication, like Gd-doping, provides little means for suppressing this background, or the correlated background caused by the time-correlated capture of two spallation neutrons, the first mimicking a slowing positron and the second the inverse beta final state neutron.

Here we describe an investigation of a detector material that can identify neutron captures and therefore reject a large fraction of those γ-ray uncorrelated and multiple neutron capture correlated background events. The material, produced by MSI Photogenics, consists of $\approx$ 1 mm shards of an inorganic scintillator distributed in a plastic scintillator matrix, loaded to 1% by weight. The inorganic scintillator $^{6}Li^{nat}_{6}Gd(^{10}BO_3)_3$:Ce (LGB), has a very high neutron capture cross section, high light output, and has an index of refection well matched to that of plastic scintillator. A detailed description of the properties of LGB inorganic scintillator can be found in [4], while the development of the material used here is described in [5]. Neutron captures on ^{6}Li or ^{10}B are relatively easy to identify via Pulse Shape Discrimination (PSD) techniques, since the resulting heavy ions are fully contained within the crystal shards and the inorganic scintillator has a relatively long ($\approx$ 200 ns) decay time, compared to the organic scintillator ($\approx$ 3 ns).

2. Detector Descriptions

Two detectors were acquired from MSI/Photogenics for this investigation. The first was a cylinder of 12 cm diameter and 12.3 cm length containing crystal shards ranging in linear dimension between 0.5 mm and 1.5 mm. The second was a cylinder of 12 cm diameter and 34.8 cm length containing crystal shards ranging in linear dimension between 1.5 mm and 3.0 mm.

Each detector was loaded with 1% by weight of LGB crystal shards. A photograph of the smaller detector is shown in Fig. 1. Clearly, the optical transmission properties of the base plastic material in the visible light spectrum are affected by the inclusion of the crystal shards and a trapped air bubble is apparent. Hamamatsu H6527 12.5 cm Photomultipler Tube (PMT) assemblies were coupled to each end of the detector cylinders using optical grease.

3. Data Acquisition System

A schematic of the QDC-based system is shown in Fig. 2a. Two copies of each PMT signal are integrated by a CAEN V792N QDC. The delay between these two copies is carefully adjusted with respect to the QDC gate so that one copy is fully integrated, while only the tail portion of the second copy is. As demonstrated in Fig. 2b this approach yields a different value for the ratio of integrated amplitudes for events with different decay constants. The full charge integral can be used for an event energy determination. This method is equivalent to implementing two different QDC gates during the charge integration of each PMT pulse. The ratio of the amplitudes ("tail/full") depends upon the

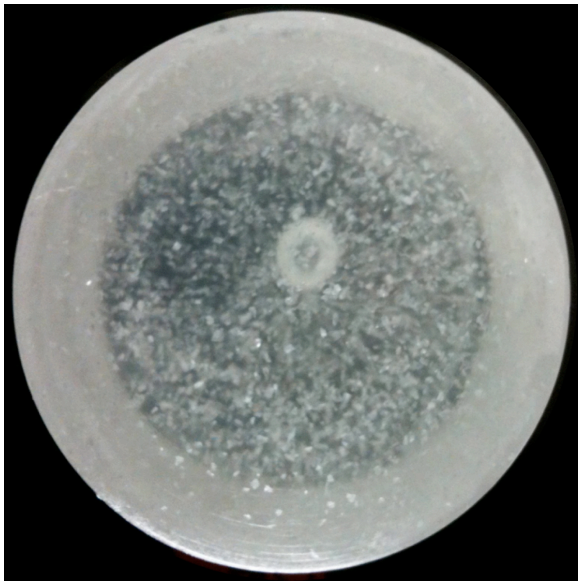

Figure 1: A photograph of the smaller of the two detectors examined. The LGB crystal shards and a trapped air bubble can be clearly seen.

decay time constant of the PMT pulse. For events occurring within the fast decaying plastic scintillator this ratio will be small, whereas for events occurring within the slow decaying LGB crystals it will be large.

4. Detector Calibration

A relationship between recorded QDC charge and electron-equivalent energy deposition in the plastic scintillator component of the two detectors was established using the 511 keV and 1275 keV γ-rays emitted by a ^{22}Na source. A "fan" collimator of lead bricks separated by a 0.4 cm gap was used to preferentially illuminate the center portion of each detector (Fig. 3). The "full" response was recorded and is plotted for each PMT and detector in Fig. 4. The energy scale was established using a GEANT4 [8] simulation of the calibration configuration (Fig. 3). The GEANT4 model incorporated randomly distributed LGB inclusions matching the average size quoted by the manufacturer and only recorded electron energy depositions. Detector resolution effects due to photo-statistics, etc, were accounted for by convolving the simulated "ideal" response with a gaussian resolution function in post-analysis. Two features corresponding to the Compton edges of the two γ-rays can be clearly observed in Fig. 4 . Detector resolutions of 15% and 25% were found, qualitatively, to be a good representation of the properties of the 12.3 cm and 34.8 cm detectors, respectively.

Using a reasonable approximation of exponential attenuation of light as it propagates through the detectors, we can combine the recorded signals of the "left" and "right" PMTs ($E_L$and E_R) to correct for interaction position dependencies in the analysis that follows. Assuming an effective attenuation length (α_{eff}), that incorporates the effect of the both non-perfect reflection at the detector boundaries and optical absorption within the detector, we can write the event energy (E) as:

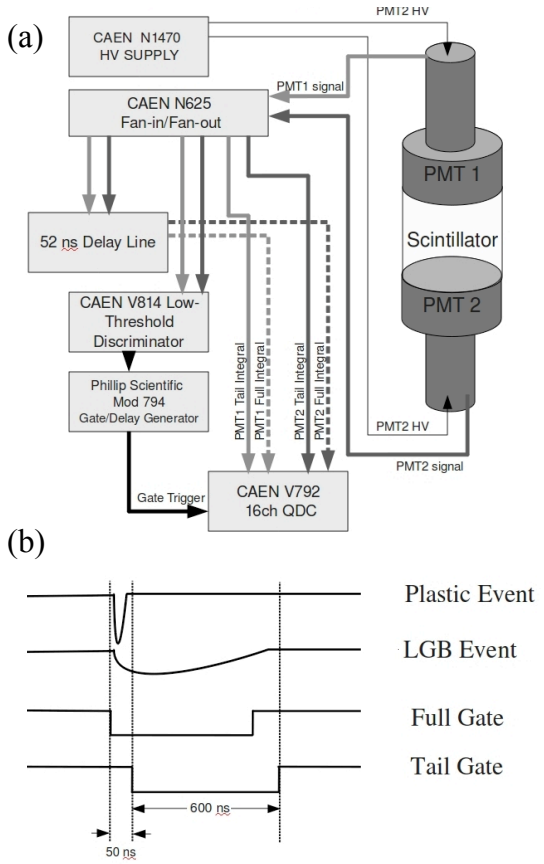

Figure 2: (a) A schematic diagram of the QDC-based DAQ system. Two copies of the PMT signal, with a relative delay, are integrated using a CAEN V792N QDC. (b) A schematic timing diagram for the QDC DAQ. Two copies of the PMTs pulses are input to the QDC with a relative delay of $\approx$ 50 ns.

$$\sqrt{E_L E_R} = \sqrt{(Ee^{-x/\alpha_{eff}})(Ee^{x/\alpha_{eff}})} = E. \quad (1)$$

That this is a reasonable approach can be seen in Fig. 5, where ^{22}Na spectra taken at several collimator positions are compared. Each is in good qualitative agreement with that taken at the center (the energy calibration position).

5. Optical Attenuation Measurements

The collimated γ-ray source used for energy calibration was also used to measure the effective optical attenuation length for each detector. The variation in the absolute position (measured in QDC channels) of the spectral features due to the 511 keV and 1.275 MeV γ-rays was recorded for each PMT from various source positions. Representative results for the "left" PMT of both detectors are shown in Fig 6 for the 511 keV feature. The inferred optical attenuation lengths are given in Table. 1. The two independent measurements made for each detector are in good agreement.

γ-ray energy	Effective Attenuation Length (cm)	
	12.3 cm detector	34.8 cm detector
511 keV	17.7 ± 2.0 cm	18.4 ± 1.2 cm
1275 keV	16.8 ± 2.0 cm	18.0 ± 1.2 cm

Table 1: Effective attenuation lengths measured for both detectors at two γ-ray energies.

The modest attenuation lengths measured suggest that this material, as currently manufactured, would not support detector lengths at the 1 m scale ideal for antineutrino detection applications. In a 1 m length detector, light from an interaction at one end of the detector would be attenuated by least 2 orders of magnitude before reaching the PMT at the other end. This would make position reconstruction and correction unreliable. However, lengths of $\approx$ 50 cm appear feasible, and might be sufficient, given the attractive neutron capture identification properties of the material.

6. Neutron Capture Identification Results

The neutron capture response of both detectors was investigated using a bare 2.5 μCi ^{252}Cf source placed 30 cm from the detector center. Plots of electron-equivalent energy aginst the PSD parameter ("tail" energy/"full" energy) from 1 hour acquisitions are displayed in Fig. 7 for the 12.3 cm detector and in Fig. 8 for the 34.8 cm detector. Background data are also shown for comparison. As can be seen, the hardware threshold of $\approx$ 75 keV was sufficiently low to record the neutron capture features of interest.

Two distinct features with PSD parameters close to unity due to neutron capture can be observed in these plots: one near an electron equivalent energy of $\approx$ 2.2 MeVee due to captures on ^{6}Li, and the other near 0.75 MeVee due to captures on ^{10}B. Note that these neutron capture features are found at considerably greater electron-equivalent energy than would be expected for doped organic scintillators ($\approx$ 500 keVee for ^{6}Li [2] and $\approx$ 50 keVee for ^{10}B [9]), since the neutron capture reaction products lose energy primarily in the inorganic LGB shards, which exhibit lower quenching. Good separation from events in the plastic scintillator is especially evident for the ^{6}Li captures. The ^{10}B capture feature spans a greater range of values in the PSD parameter, since 94% of these events are accompanied by a 478 keV γ-ray. Compton scatters of those γ-rays add to the energy of the capture event and reduce the PSD parameter value, since they increase the "full" integral value, but not the "tail" integral value.

The ^{10}B capture feature is also more difficult to distinguish from background γ-ray interactions due to its lower average energy, which is due both to the lower Q-value of the neutron capture reaction (2.3 MeV for ^{10}B versus 4.8 MeV for ^{6}Li)and the higher quenching of the heavier daughter products. Low energy Compton electrons can deposit a significant fraction of their total energy in a crystal grain, raising the measured value of the PSD parameter for those events. This effect appears to contribute a significant non-neutron background to the ^{10}B capture region.

Measurements of the neutron capture efficiency were compared to a GEANT4 simulation (Table 2). Again, the GEANT4 model incorporated randomly distributed LGB inclusions matching the average size quoted by the man-

	^{6}Li Capture Efficiency (%)	
	12.3 cm detector	34.8 cm detector
Measured	1.71 ± 0.24	1.38 ± 0.14
Simulated	1.47 ± 0.25	1.76 ± 0.25

Table 2: Measured and simulated neutron capture efficiencies upon ^{6}Li.

Isotopics	Fraction of neutrons (%)				
	^{6}Li	^{10}B	Gd	H	Escape
^{6}Li^{nat}Gd^{10}B	10.8	21.4	43.0	12.0	12.8
^{6}Li^{dep}Gd^{10}B	23.4	49.4	-	14.6	12.6
^{6}Li^{dep}Gd^{11}B	63.3	-	-	21.5	15.2
^{6}Li^{nat}Gd^{11}B	15.0	-	59.9	12.5	12.6

Table 3: The predicted fraction of neutrons that capture on particular nuclei or that escape a 1 m^3 detector. ^{dep}Gd refers to gadolinium that has been completely depleted of ^{155}Gd and ^{157}Gd.

ufacturer. The simulation simply tallied the number of neutrons captured upon ^{6}Li and ^{10}B for an incident fission neutron spectrum, but did not simulate the scintillation or optical collection properties of the system. The error on the simulated efficiency was estimated by both increasing and decreasing the LGB particle size by 50%, since the particle size distribution is unknown. The ^{10}B efficiency is not considered, since there are several reasons why the measured efficiency is unreliable. First, the relatively poor γ-ray discrimination of the ^{10}B capture feature and the multitude of high energy γ-rays emitted by ^{252}Cf made reliable neutron counting difficult with this nucleus. Second, it was noticed via inspection of oscilloscope traces that many apparent ^{10}B neutron captures did not trigger the DAQ system. This is because the triggering is based upon a voltage level discriminator - the maximum voltage of the slow ^{10}B PMT pulse is considerably lower than that of a γ-ray with an equivalent integrated PMT amplitude.

The reasonable agreement between experiment and simulation allows us to use that same simulation to estimate the neutron capture efficiency of this material for lower neutron energies ($\approx$ 10 keV) relevant to the antineutrino detection application, and to investigate the effect of varying the LGB crystal isotopic composition. Of course, any proton recoils resulting from such neutrons would be too low in energy to observe; the positron produced in the inverse beta decay interaction provides the prompt portion of the coincident signal. The GEANT4 simulation was repeated for a 1 m^3 detector with 10 keV neutrons distributed uniformly within the detector volume. The fraction of neutrons that capture on ^{6}Li, ^{10}B, Gd (^{155}Gd or ^{157}Gd), H, or that escape the detector are given in Table 3 for several different LGB isotopic compositions.

Assuming that a means could be found to reliably register all ^{10}B captures, the isotopic composition used in

this investigation would yield a total neutron capture efficiency for inverse beta-decay detection of $\approx$ 30%, similar to that of previously demonstrated antineutrino detectors for reactor monitoring [3], but far from ideal. If it were economically feasible to produce gadolinium depleted in ^{155}Gd and ^{157}Gd, very attractive capture efficiencies could be achieved. In particular, use of ^{dep}Gd and ^{11}B would be ideal, providing high efficiency for the easily identified ^{6}Li capture. Although alternate ^{6}Li bearing inorganic scintillators, e.g. $Li_6Yt(BO_3)_3$ and Li glass, have considerably lower light yield, the prospect of higher neutron capture efficiency suggests that they warrant further investigation for this application.

7. Conclusion

The composite LGB/Plastic scintillator material has many attractive features for antineutrino detection. The very good PSD separation of ^{6}Li neutron captures would provide a powerful means to reject random γ-ray coincidences. This in turn might allow for a reduction in passive shielding and a reduction in total device size—an important parameter for the reactor monitoring application. The fact that the LGB detector material is a solid plastic could have practical advantages over the more typically used liquid scintillator.

However, this material, as currently realized, also has significant drawbacks. The optical properties do not support detector elements of the desired length. Also, despite its very high neutron capture cross section, the incorporation of gadolinium in the inorganic crystal results in a reduced identifiable neutron capture efficiency. Further work to improve the manufacturing process that incorporates the crystals shards in the plastic would be beneficial.

Other avenues for future investigation include studying the effect of crystal shard size upon neutron capture efficiency and attempting to identify other suitable inorganic crystals that contain only ^{6}Li as a neutron capture agent. Finally, we note that this material would be ideal for use in a segmented capture-gated neutron spectrometer: appropriate segmentation would allow for enhanced event-by-event resolution [10], while the unambiguous neutron capture indication would provide strong background rejection.

Acknowledgements

LLNL-JRNL-482515. This work was performed under the auspices of the U.S. Department of Energy by Lawrence Livermore National Laboratory in part under Contract W-7405-Eng-48 and in part under Contract DE-AC52-07NA27344.

References

[1] J. B. Czirr and G. L. Jensen, Nucl. Inst. and Meth. A 284 (1989) 365
[2] M. Abbes, et al., Nucl. Inst. and Meth. A 284 (1996) 164
[3] N. S. Bowden, et. al., Nucl. Instr. and Meth. A. 572 (2007) 985
[4] J. B. Czirr et al., Nucl. Inst. and Meth. A 414 (1999) 15
[5] J. B. Czirr et al., Nucl. Inst. and Meth. A 476 (2002) 309

[6] M. Flaska, et al., IEEE NSS Conf. Rec. (2008) 3376
[7] N. Menaa, et al., IEEE Trans. Nucl. Sci. 56 (2009) 911
[8] S. Agostinelli et al., Nucl. Inst. and Meth. A 506 (2003) 250
[9] T. Aoyama, et. al., Nucl. Instr. and Meth. A. 333 (1993) 492
[10] N. S. Bowden, et. al., Nucl. Instr. and Meth. A. 609 (2009) 32

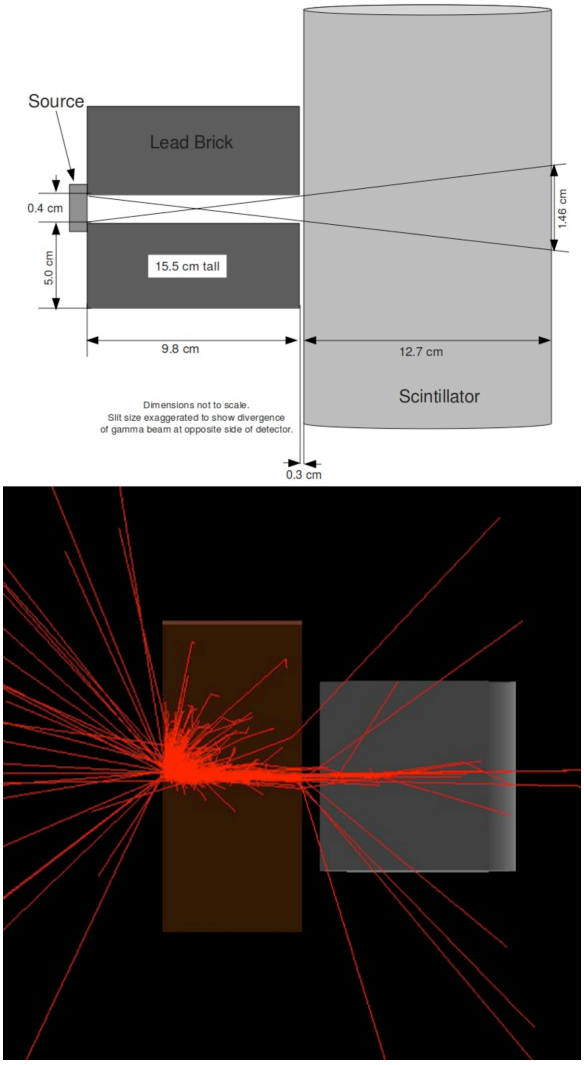

Figure 3: The dimensions and position relative to the detector(s) of the "fan" collimator used for calibration are shown, as well as a rendering of the GEANT4 implementation of the collimator (brown), detector (grey) and several gamma ray events (red).

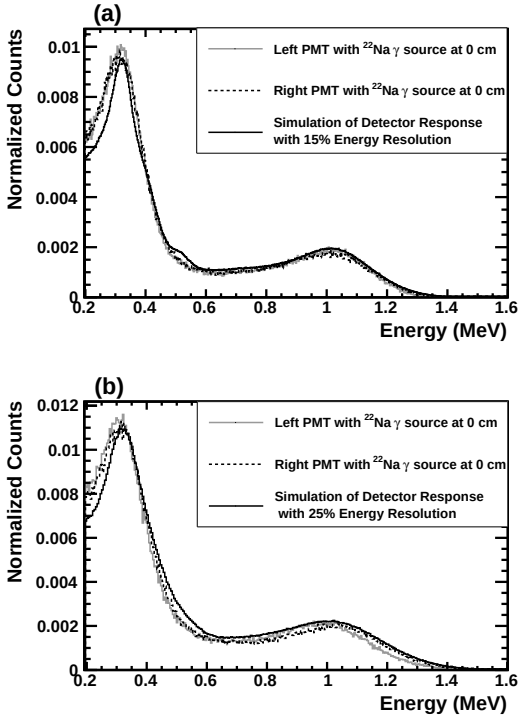

Figure 4: Calibration spectra taken with a collimated ^{22}Na source placed at the center of the (a) 12.3 cm and (b) 34.8 cm detectors is compared to the simulated response.

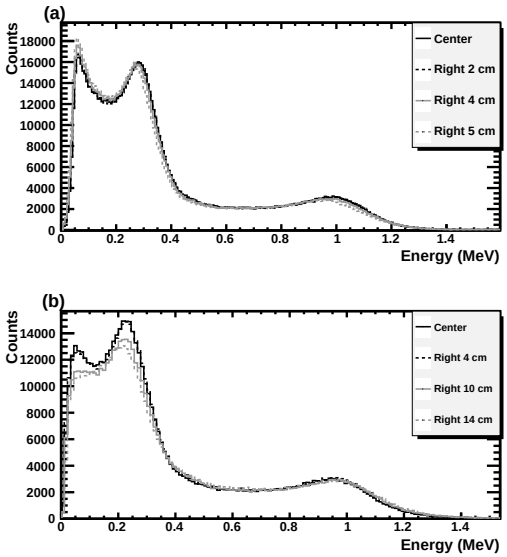

Figure 5: Spectra taken with a collimated ^{22}Na source placed at various positions relative to the center of the (a) 12.3 cm and (b) 34.8 cm detectors. The good agreement between these spectra indicates that position dependencies are largely accounted for by the appropriate combination of the two PMT amplitudes.

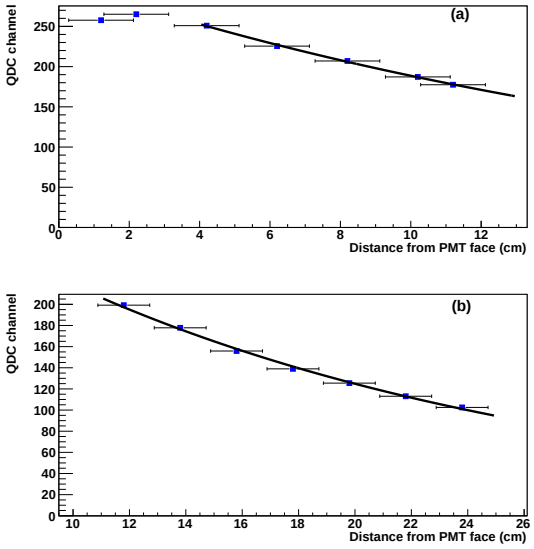

Figure 6: Relative optical intensity of the Compton edge for 511 keV γ-rays as a function of γ-ray source position. Data are shown for the (a) 12.3 cm and (b) 34.8 cm detectors.

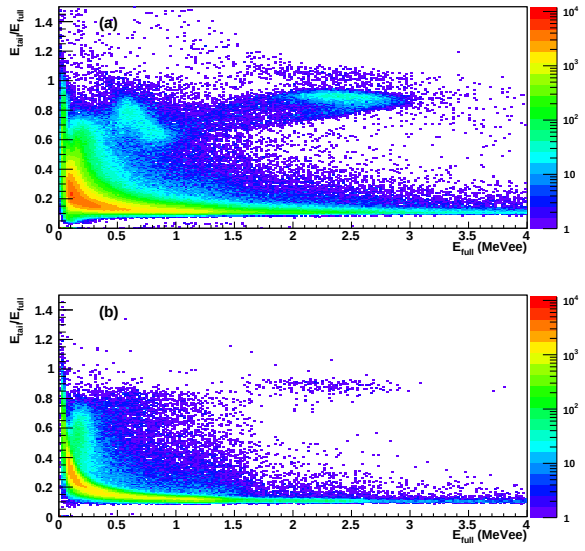

Figure 7: (a) Data demonstrating the ability of the 12.3 cm detector to identify neutron captures via PSD when irradiated by a ^{252}Cf source. (b) A background spectrum is shown for comparison.

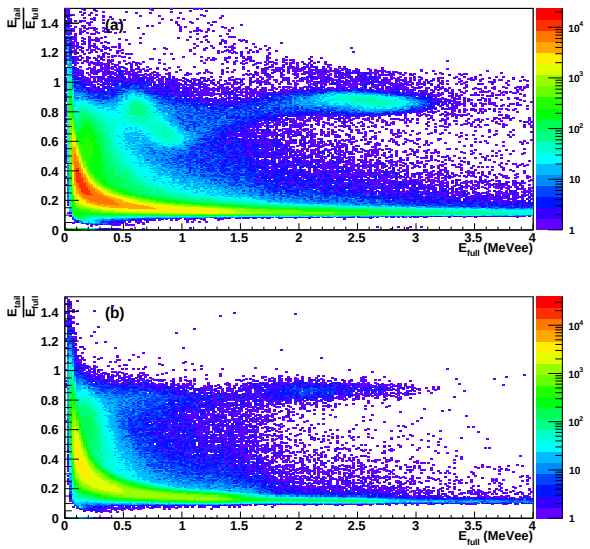

Figure 8: (a) Data demonstrating the ability of the 34.8 cm detector to identify neutron captures via PSD when irradiated by a ^{252}Cf source. (b) A background spectrum is shown for comparison.